# Bioimpedance Measurement of Avocado Fruit Using Magnetic Induction Spectroscopy

**DOI:**
10.1109/TAFE.2023.3303177

**Document Version**
Accepted author manuscript

# Bioimpedance Measurement of Avocado Fruit using Magnetic Induction Spectroscopy

Michael D. O'Toole, *Member, IEEE,* Marcin Glowacz, Anthony. J. Peyton *Member, IEEE,*

***Abstract*—Avocado fruit is a popular, nutritious and commercially valuable product that, with a short window of ripeness and heterogeneous maturity, presents particular challenges when bringing to market. There is significant value in being able to measure avocado fruit ripeness and maturity, especially non-destructively, with the prospect of improvements in consignment management, food loss, and consumer satisfaction.**

**In this paper, we explore the bioimpedance spectra of avocado fruit. Bioimpedance has been found to correlate with ripeness in avocado fruit over a frequency range termed the $\beta$-dispersion where cell polarisation effects are significant. Our contribution is to use Magnetic Induction Spectroscopy to measure conductivity across this range, an entirely non-contact method that uses eddy-currents induced in the fruit flesh by magnetic fields rather than penetrative or surface electrodes as in previous work.**

**We were able to measure a clear $\beta$-dispersion curve, finding fruit conductivity rising from $\sim$0.6 mS/cm at 100 kHz to $\sim$4 mS/cm at 10 MHz. This agrees with the literature at higher and lower frequencies, and completes a gap in the spectra not previously reported. Further, we find evidence of changes to the conductivity spectra as the fruit ages and ripens, with the spectra broadly flattening according to a set of identified trends. This indicates a relation between bioimpedance spectra and ripeness, although high inter-sample variability precludes the spectra as a direct estimation technique at this stage.**

***Index Terms*—Bioimpedance, Eddy current testing, Food technology, Non-destructive testing.**

## I. Introduction

AVOCADO fruit is an economically valuable product, favoured for its nutritional content and health benefits [1]. Over the last two decades, it has seen considerable growth in popularity, particularly in Europe and North America where combined consumption per capita has more than tripled [2]. However, avocado is a difficult fruit to market. It is highly perishable with a limited shelf-life; subject to bruising, infections, and chilling injury; and has a short window of ripeness acceptable to the consumer [3]. Heterogeneous maturity is also a problem. Avocado fruit matures on the tree but only ripens when picked. The lack of visible signs of maturity makes it difficult to decide when to harvest for optimum taste and flavour, and can lead to wide variations in age, with differing rates of ripening of the fruit across a single batch [4]–[7].

Delivering consistent maturity and ripening behaviour to the consumer is a major challenge for industry [7], [8], driving the search for more accurate, rapid and reliable tests [9]. Destructive tests, such as measuring oil fraction, dry matter and moisture content, and firmness are for the most part well correlated with maturity, quality, or ripeness [9]. However, these tests can be time-consuming and expensive. They require sampling of the fruit and assume that the measured and destroyed samples are representative of the entire batch [10]. Non-destructive methods open the possibility of wider consignment measurement, on-tree, or on-line during packaging and distribution. Non-destructive firmometers using micro-deformations have gained a degree of market acceptance [11], [12]. Optical (Vis/NIR, hyperspectral, image processing), acoustic (ultrasonic), and nuclear magnetic resonance modalities have shown some efficacy but have not achieved widespread adoption [9]. More subjective measures still prevail, such as touch [13], or colour as some varieties transition from green to dark purple during ripening [14].

The electrical properties of avocado fruit are affected by the physiological processes occurring during ripening. These properties, presented in terms such as impedance, resistance, conductivity, and permittivity amongst others, define how electric fields and current interact with the fruit tissue. In what follows, we will use the general term *bioimpedance* to describe how biological tissue such as fruit oppose the flow of electric current and use the more specific term conductivity to mean the ratio of in-phase current to the electric field, or equivalently the power loss or dissipation within the material [15].

The conductivity of avocado fruit has been shown to correlate with indicators of ripeness, such as changes in respiration, ethylene production, and firmness [16]–[21]. Conductivity was found to increase with ripeness when measured using direct current (DC) sources or when oscillating at frequencies below 60 kHz. Changes in conductivity were also observed due to chilling injury [19]. These *single frequency* measurements, however, lack selectivity and can fail to account for confounding variables such as electrode contact impedances and temperature variations [22]. An alternative is to consider *bioimpedance spectroscopy* (or conductivity as a subset), that is, measurement across a range of excitation frequencies.

The bioimpedance spectra of tissue is composed of a series of dispersions associated with different mechanisms of interaction between electric field and current-flow [23]. The $\beta$-dispersion, across the kHz-MHz range, is of interest to this study as it is caused by cell polarisation. The cell

This work was supported in part by the UK Science and Technology Facilities Council (STFC) Food Network+ Scoping project grant.

Michael. D. O'Toole and Anthony. J. Peyton are with the Department of Electrical and Electronic Engineering, The University of Manchester, UK (email: michael.otoole@manchester.ac.uk, a.peyton@manchester.ac.uk). Marcin Glowacz was with the University of Greenwich (email: glowacz.m.m@gmail.com)

walls are low or non-conductive dielectrics enclosing and surrounded by resistive intra-cellular and extra-cellular fluids. In this sense, the walls act like electrical 'capacitors', charging and discharging the surface with the applied electric field. As the fruit ripens, there is degradation in the polysaccharide components of the cell walls causing them to loosen and swell, reducing inter-cellular adhesion, becoming more hydrated and open, and eventually breaking apart [24]. Their dielectric properties inevitably change with this process, observed as a 'flattening' of the $\beta$-dispersion as ripening progresses [25]–[27]. At lower frequencies, the conductivity and permittivity of the tissue rise and fall respectively with ripeness. At higher frequencies, the cell walls present a small impedance like a capacitor, and thus the conductivity and permittivity are relatively insensitive to these physiological changes.

The bioimpedance spectra of avocado fruit has been measured using direct-contact electrodes [25]–[27] and coaxial probes [13], [28]. The $\beta$-dispersion was observed across 50 kHz to 20 MHz, although with a gap in the available data from 1 MHz to 10 MHz. This part of the dispersion curve is therefore missing to us from the overall spectra.

In this paper, we use *magnetic induction spectroscopy* to measure the bioimpedance spectra of avocado fruit. This method induces eddy-currents in the flesh of the fruit using oscillating magnetic fields emitted by an excitation coil. These eddy-currents in turn induce secondary magnetic fields measured by a receive coil. This approach is entirely non-contact: It requires no preparation to the fruit, avoids surface interface problems associated with direct-contact electrodes, and has minimal effect on the fruit as the interrogative eddy-currents are too small for bio-heating. It also works well across the 1-10 MHz bandwidth gap we identified as missing for avocado fruit in the literature. MIS has been successfully used to find the conductivity spectra of potatoes, cucumbers, tomatoes, bananas, and yeast-concentrations [29]–[31]. In previous work, we were able to demonstrate MIS for the first time at a near industrial-scale using a robust non-contact system designed to be operated on a fruit sorting-line [22], [32].

In what follows, we investigate the conductivity spectra of avocado fruits over several days using a laboratory-based MIS system. We show clear and relatively consistent trends as the fruits ripen, suggesting MIS could be a new non-destructive technique to assess ripeness or sample condition. We measure part of the $\beta$-dispersion of avocado fruit not previously reported, completing the work of Yang et al. [25], [26], Islam et al. [27] and Nelson et al. [13], [28]. To our knowledge, this work is the first to report conductivity measurement of avocado fruit using eddy-currents, and the first to observe changes in $\beta$-dispersion as the fruits age without physical contact.

## II. Method

A sample set of $N = 16$ avocado fruit (Persea americana Mill.) of cultivar 'Hass' were sourced from a supermarket chain (Tesco PLC, UK). The fruits were stored chilled and packaged in batches of four in low density polyethylene bags. All samples were initially in an unripe state, being both light green in colour and firm to the touch, with no visible defects or injury. The physical characteristics of each pack (mass, length, diameter) are summarised in table I.

TABLE I
AVOCADO FRUIT SAMPLES CHARACTERISTICS

| Pack No. | Mass (g) Av. (range) | Len. (mm) Av. (range) | Dia. (mm) Av. (range) |
|---|---|---|---|
| 1 | 110.8 (±13.0) | 75.1 (±4.6) | 54.1 (±2.7) |
| 2 | 109.8 (±12.0) | 67.7 (±2.5) | 55.8 (±3.2) |
| 3 | 103.3 (±11.0) | 72.8 (±6.6) | 53.4 (±3.7) |
| 4 | 115.5 (±7.5) | 72.8 (±6.6) | 54.7 (±1.8) |

The samples were scanned using magnetic induction spectroscopy (MIS), measuring the conductivity spectra of the food-under-test from 100 kHz to 10 MHz. The first scan was on the day of purchase. The temperatures of the fruits were allowed to normalise to room temperature over several hours prior to measurement. The MIS measurement system was run for around twenty minutes to achieve temperature stability and minimise any thermal drift. A calibration scan was first conducted. The calibration method is described in section II-D. Then each avocado fruit was scanned sequentially, taking and averaging continuous measurements over approximately five minutes for each fruit. A second calibration scan then completed the test. Between each scan (both fruit and calibration), a zero or background measurement with the sensor empty.

This procedure was run every 21-96 hours over fourteen days to obtain eleven distinct spectra for each fruit spread over the test period. Between scans, the avocado fruit were stored together at room temperature in an open crate. All samples ripened (softened and darkened) over the duration and were clearly in some state of decay by the study's end.

### A. Magnetic Induction Spectroscopy (MIS) System

The MIS measurement system was developed by the authors to measure the conductivity spectra of avocado fruits, apples, and other similar-sized foodstuffs in a non-contact way. The physical system is shown in figure 1 and a schematic shown in figure 2. It consists of the following elements: (1) a coil assembly, (2) a power amplifier, (3) low-noise amplifiers, and (4) a data acquisition system with synchronous output waveform and analogue inputs. In what follows, an overview of the system is provided, however, a more comprehensive description can be found in our previous study quantifying the performance of this system [33].

The coil assembly consists of a transmit coil, receive coils, and a reference coil. The transmit coil provides an oscillating magnetic field (excitation field) which illuminates the sample-under-test and induces eddy-currents to circulate within the sample flesh. The transmit coil is constructed of a single turn wire loop of 75 mm diameter wrapped axially near the the base of the sample. It is driven by a 100 W power amplifier (Precision Acoustics Ltd, UK), of which approximately 70 W is utilised at the lowest excitation frequency, diminishing with increasing frequency as the coil impedance increases.

The eddy-currents induced in the sample further induce a secondary magnetic field measured by the receive coils. The receive coils consist of two separate coils, each consisting of

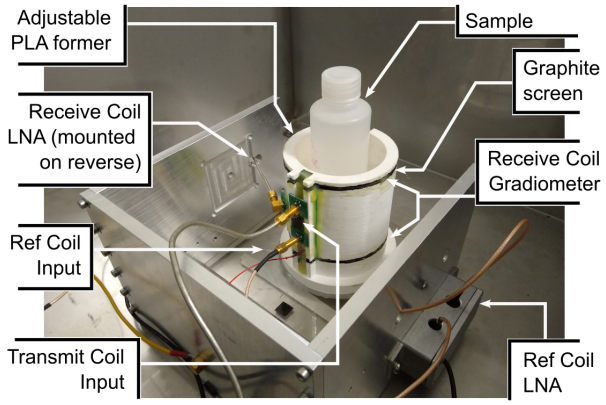


Fig. 1. Coil assembly of the magnetic induction spectroscopy system.

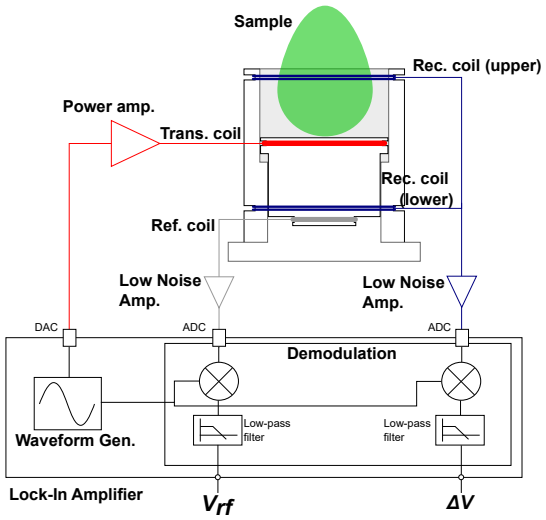


Fig. 2. Schematic of the magnetic induction spectroscopy measurement system.

two turns of diameter 85 mm, wrapped axially and situated 41.5 mm above and below the transmit coil. These two coils are connected in opposition in the manner of a gradiometer, such that any voltage EMF induced in the upper coil by the excitation magnetic field will be cancelled by the same but opposite EMF induced in the lower coil. In principle, this means that we only measure the voltage EMF induced by the secondary magnetic field emitted by the sample, and not the often much larger excitation field produced by the transmit coil. However, in practice the balance is imperfect and we can only cancel the field effects within the limits of manufacturing tolerances and system asymmetries. The receive coils are connected to a AD8099 low-noise amplifier (Analog device Inc, USA) configured in a differential circuit topology.

Finally, a reference coil consisting of a single turn of diameter 36 mm is wound axially 47 mm below the transmit coil. The purpose of the reference coil is to measure the excitation magnetic field directly and is thus located at the far end from the sample to avoid coupling of the secondary magnetic field. The reference coil is connected to an AD8099 low-noise amplifier with the same circuit configuration.

The coil assembly is set within a custom 3D-printed PLA former. The former uses a plastic spring and lead screw mechanism to fine adjust the position of the transmit coil within the receive coils gradiometer to achieve optimal balancing. The position is then secured with an epoxy-resin adhesive. The surface of the PLA former enveloping the receive coil is painted with a conductive graphite paint. This forms an near-field electric screen between the receive coils and sample-under-test, reducing the effect of capacitive coupling at higher frequencies. The coil assembly, including PLA former, is enclosed by an aluminium mount supporting the low-noise amplifiers, and further shielded by a grounded stainless steel box open only at the top for coil and sample access.

Data acquisition and waveform generation is provided by a HF2LI lock-in amplifier (Zurich Instruments, Switzerland). The system contains a synchronous 16-bit DAC output driving the power amplifier and transmit coil, and two 14-bit ADC inputs to measure and demodulate the receive coils and reference coil. The system steps sequentially through a sweep of 20 frequencies from 0.1-10 MHz, with a single sweep lasting between 5-10 seconds, returning complex components of the voltage waveforms generated in the coils at each frequency.

### *B. MIS Theory and Analysis*

Consider the case where a sample is placed in the coil assembly as shown in figure 2, and excited by a magnetic field oscillating at frequency $f$ (in Hz) or equivalently $\omega = 2\pi f$ (in rads/s) generated by the transmit coil. A voltage EMF is induced in the receive coils $V_{rx}(t)$ and the reference coil $V_{rf}(t)$. We can express these voltages in complex exponential form,

$$V_{rx}(t) = V_{rx}(\omega)e^{j\omega t}, \quad V_{rf}(t) = V_{rf}(\omega)e^{j\omega t}$$

where $j = \sqrt{-1}$ and $V_{rx}(\omega), V_{rf}(\omega)$ are complex scalars. The term $V_{rx}(\omega)$ is the superposition of the EMF induced by the excitation magnetic field and the field emitted by the object. The former is minimised by the coil gradiometer arrangement described in the previous section, however, inevitably some residual signal still remains. We may remove this residue by subtracting a background scan,

$$\Delta V(t) = \Delta V(\omega)e^{j\omega t} = (V_{rx}(\omega) - V_{bk}(\omega))e^{j\omega t}$$

where $V_{bk}(\omega)$ is the result $V_{rx}(\omega)$ from a measurement taken when the coil assembly is empty. The reference coil is situated sufficiently far from the object so as not to be affected by its field and will only measure excitation.

In what follows, we will determine the relations between material properties of the sample under test and the measured quantities, $\Delta V(\omega), V_{rx}(\omega)$. As the avocado fruit is essentially non-magnetic, with relative permeability $\mu_r = 1.0089$ [34], we use the analytical expression for a non-magnetic sphere in a uniform field [35]. Although the avocado fruit is not spherical, and the coil geometry cannot deliver a uniform field over the full sample, this simplified case can be generalised by choice of a suitable geometric correction factor [22], [29].

Consider a non-magnetic dielectric sphere of radius $a$, permittivity $\epsilon$, and conductivity $\sigma$, positioned at the origin of a cylindrical coordinate system with $\phi$, $\rho$ and, $z$ representing

the rotational, radial and longitudinal components respectively. The properties $\sigma$ and $\epsilon$ are frequency dependent $\sigma(\omega), \epsilon(\omega)$ due to the cell polarisation responsible for the $\beta$-dispersion curve. Finally, define the complex permittivity of the sample as,

$$\epsilon^* = \epsilon - j\sigma/\omega \tag{1}$$

The sphere is subject to a uniform oscillating magnetic field operating along the $z$-axis, $B_z(t) = B_z(\omega)e^{j\omega t}$. We term this the excitation magnetic field. The excitation induces eddy currents rotating about the $z$-axis, $J_\phi$. From Maxwell's equations and ohm's law, we obtain,

$$\nabla^2 J_\phi + \alpha^2 J_\phi = 0 \tag{2}$$

where $\alpha^2 = \mu_0\omega^2\epsilon^*$ and $\mu_0 = 4\pi\times10^{-7}$ is the permeability of free space. These eddy-currents induce a secondary oscillating magnetic field emitted by the sample. From Bidinosti et al. [35], the $z$-component of the resultant field (secondary and excitation) for a point outside the sphere can be determined using the following formula,

$$B_z' = B_z - B_z\frac{j_2(a\alpha)}{j_0(a\alpha)}\frac{a^3(r^2-3z^2)}{2z^5} \tag{3}$$

where $r^2 = z^2 + \rho^2$ and $j_n(a\alpha)$ represents spherical Bessel functions of the first kind. For the condition $a\alpha << 1$, i.e. ignoring wave propogation effects, we may approximate the Bessel functions by expanding about $a\alpha = 0$ and taking the first term (see Bidinosti et al. - appendix) to yield,

$$j_2(a\alpha)/j_0(a\alpha) \approx a^2\alpha^2/15 \tag{4}$$

Therefore, equation (3) simplifies to,

$$\frac{\Delta B_z}{B_z} = \frac{B_z' - B_z}{B_z} = -\frac{a^5\alpha^2(r^2-3z^2)}{30z^5} \tag{5}$$

For a receive and reference coil placed positioned co-incident with the $z$-axis, it is straightforward to show the following relation,

$$\Delta B_z(\omega)/B_z(\omega) \propto \Delta V(\omega)/V_{rx}(\omega)$$

Finally, by substituting the definition of complex permittivity in equation (1) we obtain the solution,

$$\frac{\Delta V(\omega)}{V_{rf}(\omega)} = P\omega\mu_0(\epsilon(\omega)\omega - j\sigma(\omega)) \tag{6}$$

where $P$ is a constant real value capturing the proportionality between the induced voltage and magnetic field as well as the geometric and spatial parameters specific to the sphere $a$, $r$ and $z$. The term is independent of the conductivity and permittivity of the sphere, as well as the frequency of measurement.

In this study, we investigate the conductivity of avocado fruit from MIS measurements which can now be obtained by the following formula,

$$\sigma(\omega) = -\frac{1}{P\omega\mu_0}\,\mathrm{Im}\left(\frac{\Delta V(\omega)}{V_{rf}(\omega)}\right) \tag{7}$$

We term $P$ the geometric correction factor. As previously noted, we can approximate different sample geometries other than a sphere by choosing different values to $P$. In section II-D, we will describe the process of finding a unique $P$ for each avocado fruit measured, using simulation and 3D-shape measurements of individual fruits.

### C. Calibration

A small ferrite piece is used to calibrate for magnitude and phase errors in the instrumentation. The ferrite piece is a 4 mm diameter toroid extracted from a 400 MHz wideband RF balun transformer (PWB-4-ALB Coilcraft Inc., USA). The piece has low conductivity and high permeability, both flat and real over the frequency range of interest. We may infer an idealised response from equation (6): For the measurement of a ferrite sample with $\mu_r >> 1$, the response simplifies to $\Delta V(\omega)/V_{rf}(\omega) \approx p_2$, or in other words a purely real component uniform with frequency.

Calibration is performed by scanning the ferrite piece on each test day before and after all the fruit samples are measured. The ferrite is scanned for approximately five minutes with background scans in between, following the same procedure as the individual avocado fruit. The ferrite measurements are then averaged and used to calibrate the measurements that day in the following manner,

$$M(\omega) = \left(\frac{\Delta V(\omega)}{V_{rf}(\omega)}\right)_{\text{calib.}} = \frac{(\Delta V(\omega)/V_{rf}(\omega))_{\text{uncalib.}}}{(\Delta V(\omega)/V_{rf}(\omega))_{\text{ferrite}}} \tag{8}$$

where the subscripts *uncalib.* and *ferrite* denote the uncalibrated avocado fruit and ferrite measurement respectively.

### D. Geometric Correction

A unique geometric correction factor $P$ is calculated for every individual avocado fruit measured using a numerical finite-element model constructed using CST EM Studio (Dassault Systèmes, France) low-frequency solver. The model consists of two coils, one excited with a 1 amp oscillating current at frequency 1 MHz, the second constrained to zero amps thus simulating a high impedance receive coil. The geometry of the coil pair is chosen to match the transmit-receive coil configuration in the MIS system. Note that only one half of the receive coil is modelled as it is not necessary to implement the full gradiometer in simulation. Models are typically kept small (less than 200k tetrahedrons) for convenience.

The process to obtain $P$ is summarised below:

1) Calculate a mapping constant $k$ that scales between the measured results $M(\omega)$ and the equivalent results in the simulation model, specifically the voltage induced on the simulated receive coil which we denote $V_{rx}^{\text{SIM}}$.
2) Obtain three-dimensional models of the surface geometry of each avocado fruit. These are stored as .stl files and imported into the simulation.
3) A simulation is run for each fruit model with material properties set to $\epsilon = \epsilon_0$ and conductivity $\sigma = 1$ S/m. The individual geometric correction factors can be calculated from (7) using the simulated results and mapping constant $k$,

$$P = -1/(\omega\mu_0)\,\mathrm{Im}\left(kV_{rx}^{\text{SIM}}\right) \tag{9}$$

The mapping constant $k$ remains valid for any object placed in the MIS system provided the coil geometry and settings (drive power, amplifier gain, etc) remain the same. It is found by comparing the measured and simulated results of a 125ml bottle saline solution. The saline has a known conductivity

of 0.69 S/m at 23.7 °C, measured using a Jenway 4510 conductivity meter (Cole-Parmer Ltd, UK) with a 027013 glass-bodied probe. The saline bottle is simulated as a cylinder positioned in the same relative position between the coils as in the experimental measurement.

The surface geometries of the individual avocado fruits are captured using an Einscan-SE 3D-scanner (Shining 3D, China). The 3D models are imported into the simulation and positioned in same position with respect to the coils as in the measurement system. The 3D images of the fruit take several minutes to complete, and consequently this process is most likely unsuitable for high-throughput post-harvest operation. However, geometric correction is only required to obtain absolute conductivities, reported here primarily for scientific interest. In the following section, we describe a means of using the fruit spectra to return a parameter independent of geometry, which may be of more practical use in fruit assessment.

### *E. Bioimpedance Analysis*

The $\beta$-dispersion can be understood by expressing the construct of the tissue as an equivalent circuit model. One of the simplest poses the cell as a network of a cell membrane capacitance $C_m$ and intracellular fluid resistance $R_{in}$ connected in series, in parallel with a resistor $R_{ex}$ representing extracellular fluid [36]. Deriving the admittance of this network and taking the real component yields equivalency with the frequency dependent conductivity term $\sigma(\omega)$ introduced in section II-B,

$$\sigma(\omega) = \frac{\omega^2 C_m^2 (R_{in} + R_{ex}) R_{in} R_{ex} + R_{ex}}{(\omega C_m R_{in} R_{ex})^2 + R_{ex}^2} \tag{10}$$

While more sophisticated models exist that better fit with data [36], this expression is sufficient to explain the general shape and behaviour of the dispersion. At low and high frequencies, the spectra will tend towards asymptotes at $\sigma = 1/R_{ex}$ and $\sigma = (R_{in} + R_{ex})/(R_{in}R_{ex})$ respectively. Similarly, a capacitance increase, indicative of a diminishing dielectric across the cell wall, will cause the spectra to become more 'flat' tending towards the upper asymptote.

To characterise the shape of the dispersion in a single metric, we define a parameter $P_y$ [37] as follows,

$$P_y = (M(\omega_{high}) - M(\omega_{low}))/M(\omega_{high}) \tag{11}$$

where $M$ is defined in (8), and $\omega_{high}$ and $\omega_{low}$ are arbitrarily chosen frequencies at the top of the dispersion (*high*) and some point on the curve (*low*). $P_y$ is effectively a normalised ratio between a component sensitive to changes in cell capacitance, and a high frequency component largely independent of that property. The normalisation has been shown to reduce dependency on sample size and shape in MIS [38], evidenced by (6) where the geometric factor is a constant.

## III. Results and Discussion

The conductivity spectra of each avocado fruit is measured using MIS and results size-corrected to obtain absolute conductivity using numerical simulation and 3D-scans of the fruit surface geometry. The mean average and measurement range (indicated by the error bars) for each of the four fruit packets are shown in figure 3.

There is clear evidence of a dispersion, which we suppose is the $\beta$-dispersion based on the established literature. For fresh fruit (day 0), the conductivities increased with frequency by nearly an order of magnitude, from approximately 0.5-0.7 mS/cm at the lowest frequency to 3-5 mS/cm at the highest. This is in contrast to the flat responses for constant conductivity saline solutions measured in our earlier study [33]. Some of these results are reproduced in figure 4 for convenience, showing comparisons of salines of known conductivity in different vessel sizes with estimated conductivity using MIS and the size correction method. Uniform responses are shown for each saline to within $\pm$0.07 mS/cm for the frequency range 0.1-5 MHz, rising to $\pm$0.26 mS/cm when including 10 MHz. The slight deviation at the higher frequencies is likely caused by the capacitive coupling between sample and coil array, which appears to have been only partly mitigated at this frequency by the graphite paint. The occurrence of capacitive coupling in MIS systems and the need for electric screening at higher frequencies is well documented [39]. Nevertheless, the scale of non-uniformity is much smaller than the changes observed in the conductivity spectra, and it is clear that we are measuring the dispersion as a property of the sample and not as an error of the instrumentation.

The results in figure 3 broadly agree with those reported in the literature. Nelson [28] and Wang et al. [40] measured the complex permittivity of avocado fruit above 10 MHz using an open-ended coaxial probe. These results are compared to the present work in figure 5. Conversion from relative complex permittivity $\epsilon_r^*$ to conductivity was via the following,

$$\sigma = -2\pi f \epsilon_0 \operatorname{Im}(\epsilon_r^*) \tag{12}$$

where $\epsilon_0$ is the permittivity of free-space. The match with Nelson is remarkable with less than 0.5 mS/cm mismatch between measurements at 10 MHz. The results from Wang et al. disagree however, with recorded conductivity of 9.89 mS/cm, more than double our own result of 3.94 mS/cm. In both cases, a decline in the gradient with respect to frequency is evident. Specifically, the conductivity spectra appears to plateau above 10 MHz suggesting this bandwidth marks the upper-end of the $\beta$-dispersion. This conforms with our own result which shows a gradual curve at higher frequencies tending towards the plateau. Again, the comparison here with Nelson is striking.

At the opposite end of the dispersion, Yang et al. [25] and Islam et al. [27] have measured impedance spectra for avocado fruit down to 50 Hz. These results are not presented here as comparable absolute conductivities cannot be obtained without knowing the electrode geometry and inter-facial characteristics. However, the shape of the spectra is instructive: Converting from impedance to admittance and considering the real component gives equivalency with conductivity for comparison. Islam et al. found a relatively linear trend with increasing conductivity over a narrow bandwidth between 50-150 Hz. Yang et al. on the other hand showed a clear curve indicating that the bottom of the dispersion, or where the conductivity curve plateaus, is around 10 kHz. This suggests

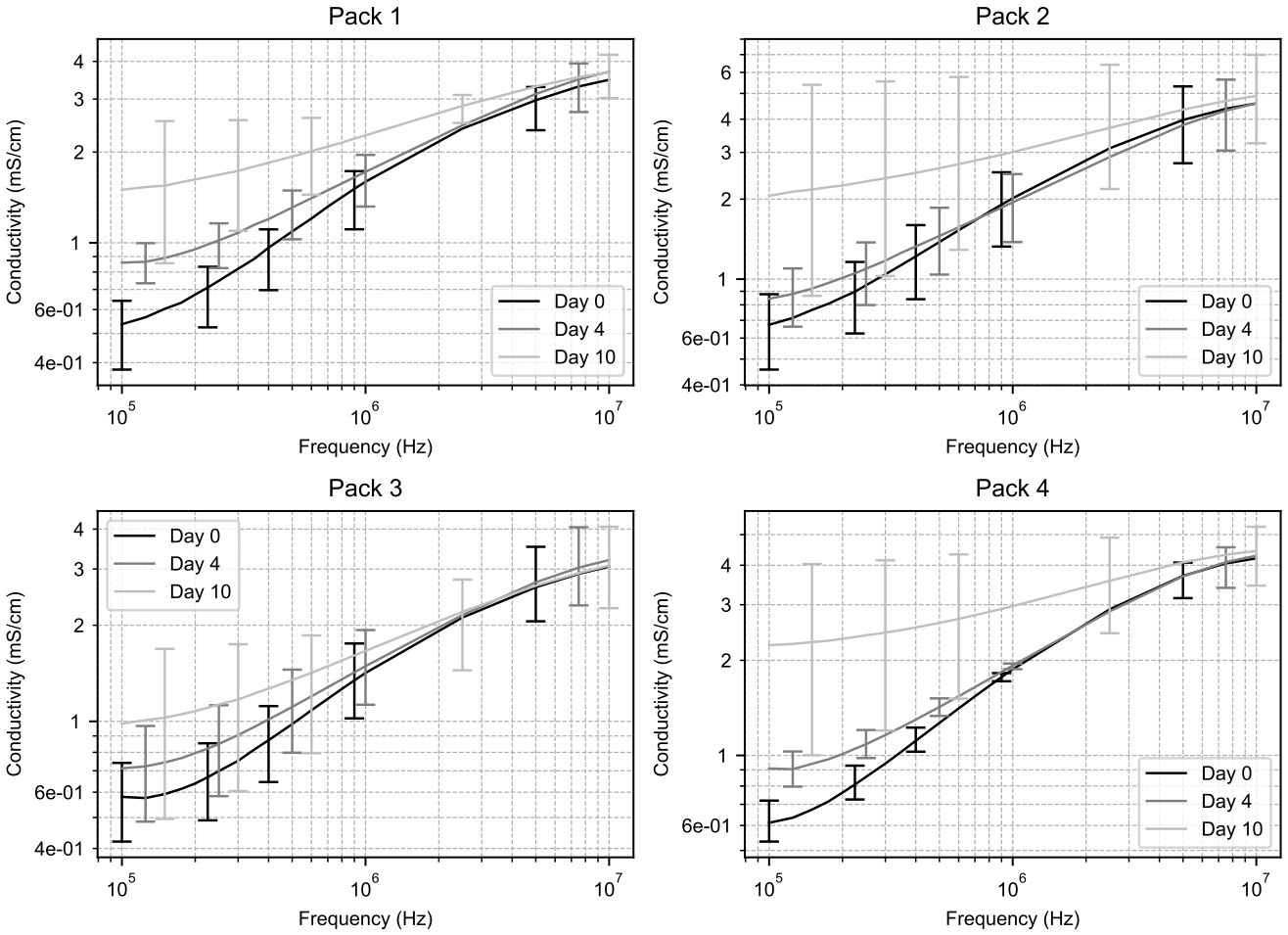


Fig. 3. Conductivity spectra of avocado fruit from 0.1-10 MHz measured using MIS. The graphs show the mean average conductivity spectra for each pack of four fruits, measured on Day 0 (day of purchase, under-ripe), day 4 (ripe) and day 10 (over-ripe). The error bars indicate the range across the pack.

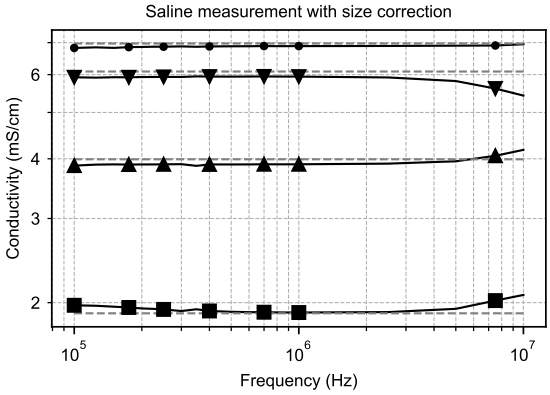


Fig. 4. MIS measurements of known-conductivity saline solutions in different vessels. Dashed lines (–) show the true conductivity of the saline.

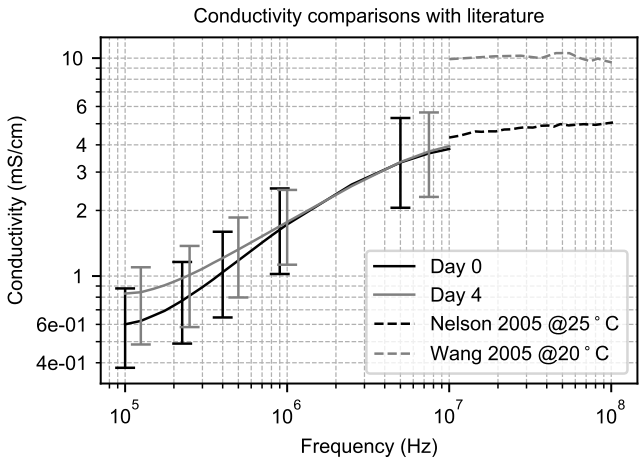


Fig. 5. Mean average conductivity spectra of avocado fruit measured by MIS compared to similar results from Nelson [28] and Wang et al. [40]

we are a frequency decade short of the full $\beta$-dispersion for avocado fruit, which appears to range from 10 kHz to 10 MHz.

Figure 3 also shows the mean conductivity spectra of the fruit packs on different days. Day 0 is the day of purchase and corresponds to the fruit being in an unripe state, day 4 a ripe state, and day 10 is overripe, assessed qualitatively by appearance (colour) and touch (firmness). Across each pack, a clear trend of flattening with frequency, or reduced gradient

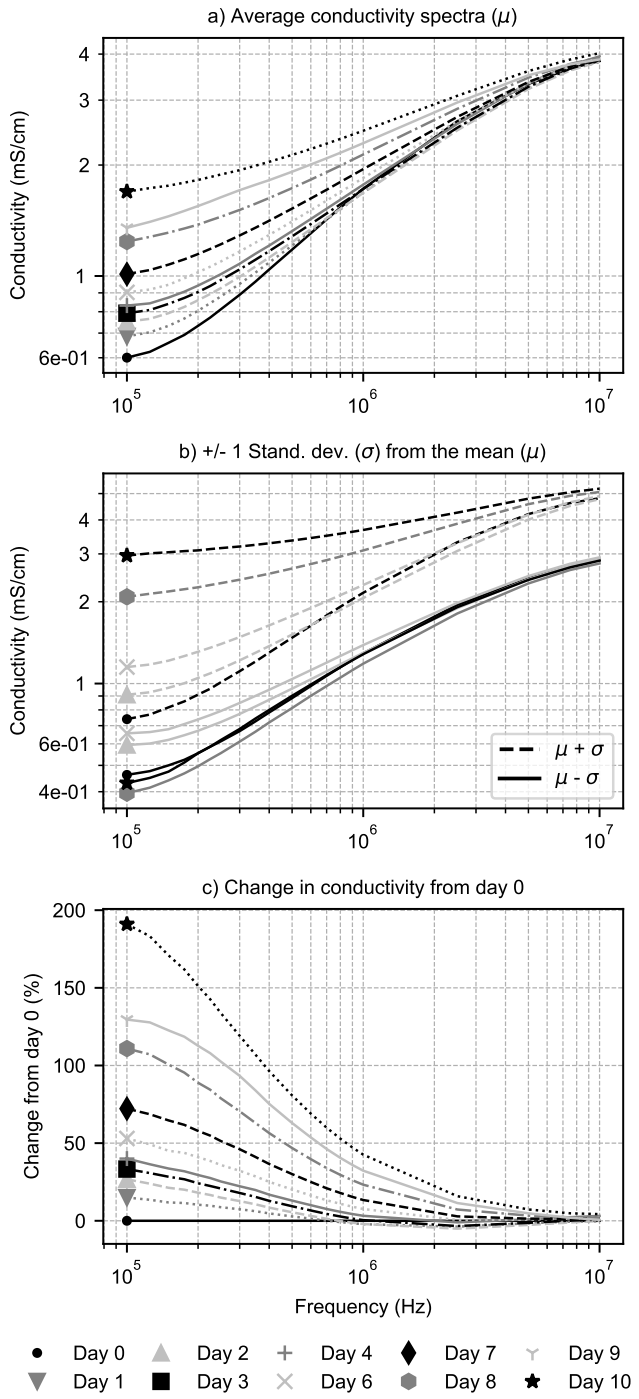


Fig. 6. Mean average conductivity results across all avocado fruit samples. Note that b) includes selected days only for clarity.

of the spectra is observed as the fruit ages. The conductivity at 100 kHz moves from between 0.5-0.7 mS/cm on day 0 to approximately 1-2 mS/cm on day 10. By contrast, the change at 10 MHz is less than 7%.

To further illustrate, the mean average conductivity across all avocado fruits is shown in figure 6 a). The dispersion curve clearly flattens with the ageing fruit, pivoting around the high frequency point of the spectra from an average 0.6 mS/cm at 100 kHz on the first day to 1.7 mS/cm on the last, progressing in order with the number of days. However, figure 6 b) shows the result +/-1 standard deviation from the mean. The variation across the samples is clearly significant. We return to inter-sample variability later in this discussion. Finally, 6 c) shows the mean average percentage change in conductivity from the first measurement. At 100 kHz, conductivity changes by 15% over the first day to 191% over the full 10 days, again progressing in order with the number of days. The average change at 10 MHz is less than 5%. This follows our understanding of the $\beta$-dispersion, where the higher frequency components are less affected by the physiological changes at the cell boundaries associated with ripening.

This pattern of spectral flattening as the fruits age is confirmed by the literature; Islam et al. [27] found the flattening of the spectra as the fruit progressed from unripe to overripe, and Yang et al. [26] associated sample resistance at 50 kHz with firmometer readings, showing decreasing resistance (increased conductivity) as the fruit softened. This pattern agrees generally with ripeness and maturation studies of different fruits, including nectarines [41], garut citrus [42], bananas [43], and mango [44], although specific trends can be more complex.

We now examine how the conductivity spectra changes over time for each fruit. In section II-E, we defined the $P_y$ parameter (equation (11)) as a ratio of conductivity change with respect to frequency, characterising the shape of the spectra within a single metric. Figure 7 shows the $P_y$ parameter calculated for each fruit at 21-96 hour intervals. The results are divided in to three different trends: Trend 1 shows declining $P_y$ over the first 3 days, followed by 4 days of little change (static period), followed by a steeper drop over the remaining time. Trend 2 is similar; there is a fall in $P_y$ over the first 2-3 days, a short static period of around 2-4 days, followed by a drop more substantial than in trend 1. Qualitatively, the initial drop, static period, and further drop phases roughly approximate to the unripe, ripe and ripeness states of the avocado fruit. Finally, in trend 3 there is an initial drop in $P_y$ over the first few days followed by a static period. Here, there is more variation than the other trends, with no further drop in $P_y$ afterwards. The proportion of fruits that fall within each trend are 6, 5, and 5 for trends 1, 2 and 3 respectively. It is unclear what aspects of the fruit are responsible for the different trends. There was no correlation for example, with the pack of origin or in physical properties such as mass and length. However, in general we find that $P_y$ dropped, meaning the conductivity spectra flattened, within the first 2-4 days followed by a further drop for most fruits 5-7 days after purchase.

Figure 7 also shows the degree of variability in $P_y$ between the different fruits. In many cases, this variability is greater than the scale of the features described by the trends, a result also noted in figure 6. For instance, the initial drop associated with unripe-to-ripe transition can be smaller than the range across the samples. This inter-sample variability leads to relatively poor Pearson and Spearman correlation coefficients of 0.54 and 0.63 respectively ($p < 0.01$). It is difficult therefore, to apply $P_y$ directly as an estimate of ripeness or maturity despite a relatively consistent general trend having been established for individual fruits.

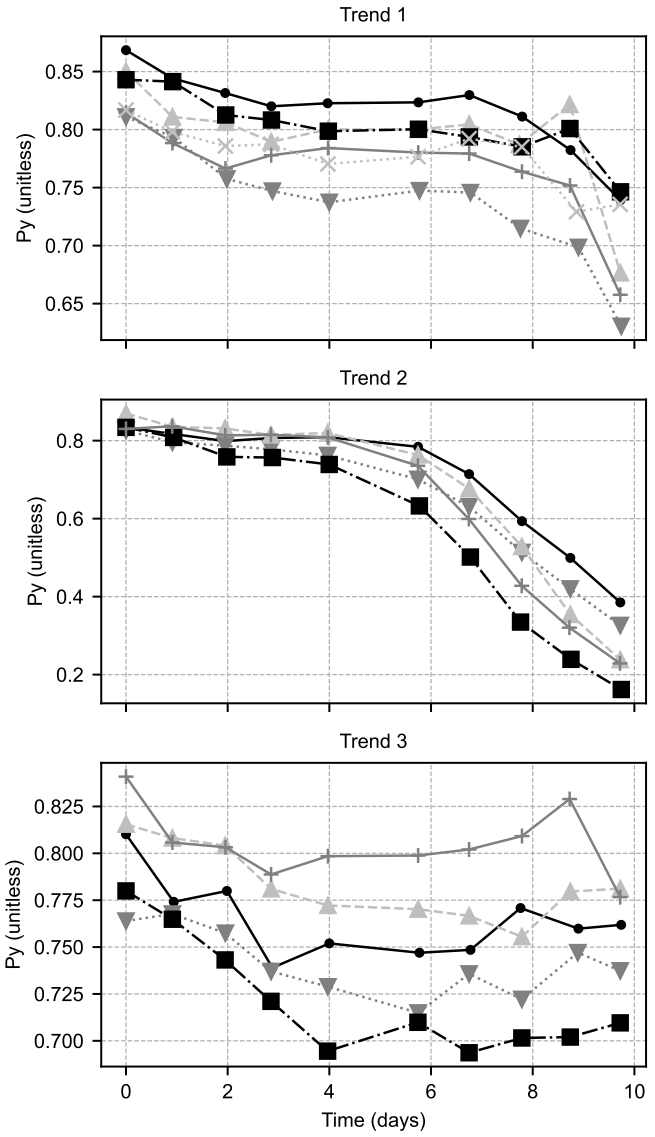


Fig. 7. $P_y$ parameter of each avocado fruit measured at 21-96 hour interval over 10 days. Results are divided across three trends, with combination of marker and line style denoting different fruit.

## IV. Conclusion

The bioimpedance spectra of avocado fruits was examined using *magnetic induction spectroscopy* (MIS); a technique with the significant advantage that it needs no direct contact with the fruit. Rather than using contact or invasive electrodes, as is common in the prior-art, MIS uses a changing magnetic field to excite eddy-currents in the sample flesh, then measures the resultant magnetic field induced by those eddy-currents. Removing the electrodes excludes the sometimes complex electrodynamic effects at the electrode-tissue interface. Further, without the need to physically penetrate the sample with electrodes, we may explore longitudinal changes in bioimpedance, leaving the fruit uninjured and intact for continued measurement at multiple different time intervals.

MIS was able to successfully measure the bioimpedance spectra over a frequency range of 0.1-10 MHz. Clear curves were obtained associated with the $\beta$-dispersion; a phenomena caused by cell polarisation in the tissue. The dispersion curves agreed with those obtained in the literature, and filled a gap in the spectra between studies using contact impedance methods limited to low frequencies, and those using higher frequency microwave methods such open-ended coaxial probes.

Avocado fruits were measured over several days to explore the relation between bioimpedance, and ripening and maturation. Introducing a single parameter ($P_y$) to describe the shape of the spectra, we identified trends that appear to match the physiological state of the fruit over time (unripe, ripe, over-ripe), implying the possibility of ripeness estimation with a non-contact technology. However, although the trends were clear for each individual fruit, the unaccounted for inter-sample variability limits the ability of this approach, at least at the present time. Accounting for this sample variability is therefore, an important consideration for future research.

## References

[1] R. G. Araújo, R. M. Rodriguez-Jasso, H. A. Ruiz, M. M. E. Pintado, and C. N. Aguilar, "Avocado by-products: Nutritional and functional properties," *Trends in Food Science & Tech.*, vol. 80, pp. 51–60, 2018.

[2] G. Naamani, "Global trends in main avocado market," in *Proceedings of the VII World Avocado Congress*, 2011.

[3] J. Gamble, F. R. Harker, S. R. Jaeger, A. White, C. Bava, M. Beresford, B. Stubbings, M. Wohlers, P. J. Hofman, R. Marques *et al.*, "The impact of dry matter, ripeness and internal defects on consumer perceptions of avocado quality and intentions to purchase," *Postharvest biology and technology*, vol. 57, no. 1, pp. 35–43, 2010.

[4] C. E. Lewis, "The maturity of avocados—a general review," *Journal of the Science of Food and Agriculture*, vol. 29, no. 10, pp. 857–866, 1978.

[5] R. Pedreschi, P. Muñoz, P. Robledo, C. Becerra, B. G. Defilippi, H. van Eekelen, R. Mumm, E. Westra, and R. C. de Vos, "Metabolomics analysis of postharvest ripening heterogeneity of 'hass' avocadoes," *Postharvest biology and technology*, vol. 92, pp. 172–179, 2014.

[6] C. Fuentealba, I. Hernández, J. Olaeta, B. Defilippi, C. Meneses, R. Campos, S. Lurie, S. Carpentier, and R. Pedreschi, "New insights into the heterogeneous ripening in hass avocado via lc–ms/ms proteomics," *Postharvest Biology and Technology*, vol. 132, pp. 51–61, 2017.

[7] S. A. Rivera, R. Ferreyra, P. Robledo, G. Selles, M. L. Arpaia, J. Saavedra, and B. G. Defilippi, "Identification of preharvest factors determining postharvest ripening behaviors in 'hass' avocado under long term storage," *Scientia horticulturae*, vol. 216, pp. 29–37, 2017.

[8] R. Nelson, "Quality challenges facing the south african avocado industry–an overview of the 2009 south african avocado season," *S. African Avocado Growers' Assoc. Yearbook*, vol. 33, pp. 7–13, 2010.

[9] L. S. Magwaza and S. Z. Tesfay, "A review of destructive and non-destructive methods for determining avocado fruit maturity," *Food and bioprocess technology*, vol. 8, no. 10, pp. 1995–2011, 2015.

[10] P. Hofman and M. Jobin-Decor, "Effect of fruit sampling and handling procedures on the percentage dry matter, fruit mass, ripening and skin colour ofhass' avocado," *The Journal of Horticultural Science and Biotechnology*, vol. 74, no. 3, pp. 277–282, 1999.

[11] F. García-Ramos, C. Valero, I. Homer, J. Ortiz-Cañavate, and M. Ruiz-Altisent, "Non-destructive fruit firmness sensors: a review," *Spanish Journal of Agricultural Research*, vol. 3, no. 1, pp. 61–73, 2005.

[12] J. Köhne, S. Kremer-Köhne, and S. Gay, "Non-destructive avocado fruit firmness measurement," *South African Avocado Growers' Association Yearbook*, vol. 21, pp. 19–21, 1998.

[13] S. Nelson, "Frequency–and temperature–dependent permittivities of fresh fruits and vegetables from 0.01 to 1.8 ghz," *Transactions of the ASAE*, vol. 46, no. 2, p. 567, 2003.

[14] K. A. Cox, T. K. McGhie, A. White, and A. B. Woolf, "Skin colour and pigment changes during ripening of 'hass' avocado fruit," *Postharvest Biology and Technology*, vol. 31, no. 3, pp. 287–294, 2004.

[15] O. G. Martinsen and S. Grimnes, *Bioimpedance and bioelectricity basics*. Academic press, 2011.

[16] R. C. Bean, J. P. Rasor, G. G. Porter *et al.*, "Changes in electrical characteristics of avocados during ripening," *California Avocado Society*, vol. 44, pp. 75–78, 1960.

[17] D. M. Ahmed, A. R. Yousef, H. Hassan *et al.*, "Relationship between electrical conductivity, softening and color of fuerte avocado fruits during ripening," *Agriculture and Biology Journal of North America*, vol. 1, no. 5, pp. 878–885, 2010.
[18] V. Hershkovitz, S. I. Saguy, and E. Pesis, "Postharvest application of 1-mcp to improve the quality of various avocado cultivars," *Postharvest biology and technology*, vol. 37, no. 3, pp. 252–264, 2005.
[19] M. Montoya, J. De La Plaza, and V. López-Rodriguez, "Electrical conductivity of avocado fruits during cold storage and ripening," *LWT-Food Science and Technology*, vol. 27, no. 1, pp. 34–38, 1994.
[20] M. Montoya, V. Lopez-Rodriguez, and J. De La Plaza, "An improved technique for measuring the electrical conductivity of intact fruits," *LWT-Food Science and Technology*, vol. 27, no. 1, pp. 29–33, 1994.
[21] M. Montoya, J. De La Plaza, and V. Lopez-Rodriguez, "Relationship between changes in electrical conductivity and ethylene production in avocado fruits," *LWT-Food Science and Technology*, vol. 27, no. 5, pp. 482–486, 1994.
[22] M. D. O'Toole, L. A. Marsh, J. L. Davidson, Y. M. Tan, D. W. Armitage, and A. J. Peyton, "Non-contact multi-frequency magnetic induction spectroscopy system for industrial-scale bio-impedance measurement," *Measurement Science and Technology*, vol. 26, no. 3, p. 035102, 2015.
[23] C. Gabriel, S. Gabriel, and y. E. Corthout, "The dielectric properties of biological tissues: I. literature survey," *Physics in medicine & biology*, vol. 41, no. 11, p. 2231, 1996.
[24] D. Brummell, "Primary cell wall metabolism during fruit ripening," *New Zealand Journal of Forestry Science*, vol. 36, no. 1, p. 99, 2006.
[25] S. Yang, I. Hallett, R. Rebstock, H. E. Oh, R. Kam, A. B. Woolf, and M. Wong, "Cellular changes in "hass" avocado mesocarp during cold-pressed oil extraction," *Journal of the American Oil Chemists' Society*, vol. 95, no. 2, pp. 229–238, 2018.
[26] S. Yang, I. Hallett, H. E. Oh, A. B. Woolf, and M. Wong, "The impact of fruit softening on avocado cell microstructure changes monitored by electrical impedance and conductivity for cold-pressed oil extraction," *Journal of Food Process Engineering*, vol. 42, no. 4, p. e13068, 2019.
[27] M. Islam, K. Wahid, and A. Dinh, "Assessment of ripening degree of avocado by electrical impedance spectroscopy and support vector machine," *Journal of food quality*, vol. 2018, 2018.
[28] S. O. Nelson, "Dielectric spectroscopy of fresh fruit and vegetable tissues from 10 to 1800 mhz," *Journal of Microwave Power and Electromagnetic Energy*, vol. 40, no. 1, pp. 31–47, 2005.
[29] A. Barai, S. Watson, H. Griffiths, and R. Patz, "Magnetic induction spectroscopy: non-contact measurement of the electrical conductivity spectra of biological samples," *Measurement Science and Technology*, vol. 23, no. 8, p. 085501, jun 2012.
[30] J. Tang, W. Yin, and M. Lu, "Bio-impedance spectroscopy for frozen-thaw of bio-samples: Non-contact inductive measurement and finite element (fe) based cell modelling," *Journal of Food Engineering*, vol. 272, p. 109784, 2020.
[31] Z. Zhang, M. A. Roula, and R. Dinsdale, "Magnetic induction spectroscopy for biomass measurement: A feasibility study," *Sensors*, vol. 19, no. 12, p. 2765, 2019.
[32] M. D. O'Toole, L. A. Marsh, J. L. Davidson, Y. Tan, D. W. Armitage, and A. J. Peyton, "Rapid non-contact relative permittivity measurement of fruits and vegetables using magnetic induction spectroscopy," in *2015 IEEE Sensors Applications Symposium (SAS)*. IEEE, 2015, pp. 1–6.
[33] M. D. O'Toole, W. Yin, and A. J. Peyton, "Model-based calibration of a magnetic induction spectroscopy system for absolute conductivity measurement," in *2020 IEEE Sensors Applications Symposium (SAS)*, 2020, pp. 1–6.
[34] Y. Tan, Y. Jin, N. Yang, Z. Wang, Z. Xie, X. Xu, Z. Jin, X. Liao, and H. Sun, "Influence of uniform magnetic field on physicochemical properties of freeze-thawed avocado puree," *RSC Adv.*, vol. 9, pp. 39 595–39 603, 2019.
[35] C. Bidinosti, E. Chapple, and M. Hayden, "The sphere in a uniform rf field—revisited," *Concepts in Magnetic Resonance Part B: Magnetic Resonance Engineering*, vol. 31B, no. 3, pp. 191–202, 2007.
[36] S. Abasi, J. R. Aggas, G. G. Garayar-Leyva, B. K. Walther, and A. Guiseppi-Elie, "Bioelectrical impedance spectroscopy for monitoring mammalian cells and tissues under different frequency domains: A review," *ACS Measurement Science Au*, vol. 2, no. 6, pp. 495–516, 2022.
[37] U. Pliquett, M. Altmann, F. Pliquett, and L. Schöberlein, "Py—a parameter for meat quality," *Meat science*, vol. 65, no. 4, pp. 1429–1437, 2003.
[38] M. D. O'Toole, R. J. Colgan, A. Anvar, and A. J. Peyton, "Non-contact assessment of apple condition using magnetic induction spectroscopy: Preliminary results and indications," in *2021 IEEE International Workshop on Metrology for Agriculture and Forestry (MetroAgriFor)*. IEEE, 2021, pp. 135–139.
[39] D. Špikić, M. Švraka, and D. Vasić, "Effectiveness of electrostatic shielding in high-frequency electromagnetic induction soil sensing," *Sensors*, vol. 22, no. 8, p. 3000, 2022.
[40] S. Wang, M. Monzon, Y. Gazit, J. Tang, E. Mitcham, and J. Armstrong, "Temperature-dependent dielectric properties of selected subtropical and tropical fruits and associated insect pests," *Transactions of the ASAE*, vol. 48, no. 5, pp. 1873–1881, 2005.
[41] F. Harker and J. Dunlop, "Electrical impedance studies of nectarines during coolstorage and fruit ripening," *Postharvest biology and technology*, vol. 4, no. 1-2, pp. 125–134, 1994.
[42] J. Juansah, I. Budiastra, K. Dahlan, and K. Seminar, "Electrical properties of garut citrus fruits at low alternating current signal and its correlation with physicochemical properties during maturation," *International journal of food properties*, vol. 17, no. 7, pp. 1498–1517, 2014.
[43] M. Soltani, R. Alimardani, and M. Omid, "Evaluating banana ripening status from measuring dielectric properties," *Journal of Food Engineering*, vol. 105, no. 4, pp. 625–631, 2011.
[44] M. Rehman, B. A. Abu Izneid, M. Z. Abdullah, and M. R. Arshad, "Assessment of quality of fruits using impedance spectroscopy," *International journal of food science & technology*, vol. 46, no. 6, pp. 1303–1309, 2011.

## V. Biography Section

**Michael D. O'Toole** received the MEng (Hons.) degree in Integrated engineering from the University of Reading in 2006, and Ph.D. from Loughborough University in 2011. He was a Research Associate at The University of Manchester from 2011 to 2016 working on magnetic induction systems for non-destructive inspection. He was awarded a Leverhulme Trust Early Career Research Fellowship in 2016, and appointed lecturer in 2020. He is author and co-author of over 20 scientific publications and one patent. His research interests include signal processing, and sensor and instrumentation design, with a particular emphasis on magnetic induction systems for non-destructive testing.

**Marcin Glowacz** received the MSc in Ecology from Lancaster University and PhD in Plant Biochemistry from Harper Adams University. He was appointed Research Fellow at the University of Greenwich in 2013 and Lecturer in Postharvest Technology in 2015. His expertise is in plant physiology and biochemistry, and supply chains, mostly in collaboration with industrial partners. In 2016 he was awarded DST-NRF Fellowship through the UK-South Africa Newton Fund leading to collaboration with the South African Avocado Growers' Association. He has since been appointed Senior Research Officer at Massey University.

**Anthony J. Peyton** received the BSc and PhD from UMIST in 1983 and 1986, respectively. He was appointed Principal Engineer at Kratos Analytical Ltd. in 1989, developing precision electronic instrumentation for magnetic sector and quadrupole mass spectrometers. He returned to UMIST as Lecturer working with the Process Tomography Group. He moved to Lancaster University in 1996 as Senior Lecturer. Since 2004, he has been a Professor of Electromagnetic Tomography Engineering at the University of Manchester. He has been a Principal Investigator of many national and industry funded projects and partner in ten previous EU projects. He is a co-author on over 110 journal papers, two books, and 12 patents in areas related to electromagnetics and tomography.